Free-surface aeration and momentum exchange at a bottom outlet

Aération de surface libre et échange de quantités de mouvement dans un rejet de fond

L. TOOMBES, *Connell Wagner, 433 Boundary St, Spring Hill 4000, Australia (Formerly: Department of Civil Engineering, The University of Queensland, Brisbane 4072, Australia)*

H. CHANSON, MIAHR, Reader, *Department of Civil Engineering, The University of Queensland, Brisbane QLD 4072, Australia. Fax: (+61 7) 33 65 45 99; e-mail: h.chanson@uq.edu.au*

ABSTRACT

This study aims to provide some new understanding of the air–water flow properties in highvelocity water jets discharging past an abrupt drop. Such a setup has been little studied to date despite the relevance to bottom outlets. Downstream of the step brink, the free-jet entrains air at both upper and lower air–water interfaces, as well as along the sides. An air–water shear layer develops at the lower nappe interface. At the lower nappe, the velocity redistribution was successfully modelled and the velocity field was found to be similar to that in two-dimensional wake flow. The results highlighted further two distinct flow regions. Close to the brink ($We_x < 5000$), the flow was dominated by momentum transfer. Further downstream ($We_x > 5000$), a strong competition between air bubble diffusion and momentum exchanges took place.

RÉSUMÉ

Cette étude vise à fournir un certain nouvel éclairage sur les propriétés de l'écoulement de jets à grande vitesse débitant dans une chute brutale. Une telle configuration a été peu étudiée jusqu'ici bien que visiblement liée aux rejets de fond. En aval du bord du seuil, le jet libre entraîne de l'air aux interfaces air–eau supérieures et inférieures , ainsi que le long des côtés. Une couche de cisaillement air–eau se développe à l'interface inférieure de la nappe. Sur la nappe inférieure, la redistribution de vitesse a été modélisée avec succès et le champ de vitesse s'est avéré semblable à celui de l'écoulement bidimensionnel de sillage. Les résultats montrent de plus deux régions distinctes d'écoulement. Près du bord ($We_x < 5000$), l'écoulement est dominé par le transfert de quantités de mouvement. Plus en aval ($We_x > 5000$), la diffusion des bulles d'air et les échanges de quantités de mouvement se disputent la prépondérance.

Keywords: Water jets, free-surface aeration, momentum exchange, bottom outlet, air–water flow measurements.

1 Introduction

High-velocity free-surface flows are extremely turbulent flows, and interfacial aeration is commonly observed (i.e. "white waters"). A typical example is a bottom outlet when a high-velocity supercritical flow discharges past an abrupt drop (Fig. 1). In Fig. 1, the high turbulence evidenced by the strong interfacial aeration corresponds to a flow Reynolds number of about 8 E+8. In large dams, bottom outlets are commonly used for reservoir drawdown, sediment flushing, river diversion and environmental flow releases (Vischer and Hager, 1998; Novak *et al.*, 2001).

This study aims to provide some new understanding of the air–water flow properties in high-velocity water jets discharging downstream of an abrupt drop (Fig. 2). New experimental investigations were conducted systematically downstream of the drop. The results are compared with analytical solutions of the air bubble diffusion equation and with a wake flow model. The results

explain past and present experimental trends, and they provide new insights into the interactions between the high-velocity water jet and the surrounding air.

1.1 Bibliographic review

Bottom outlets are characterized by high-velocity flows. Speerli (1999) studied the air entrainment of open channel outlet tunnels, but little research has been conducted systematically in the air–water flow properties of the high-velocity waters discharging at the downstream end of the tunnel (Ervine and Falvey, 1987; Ervine, 1998). Experimental studies of high-velocity water jets discharging into the atmosphere were often limited to visual observations (Kawakami, 1973), with a few specific studies of circular water jets (Dodu, 1957; Heraud, 1966). Some researchers performed air concentration distribution measurements (Shi *et al.*, 1983; Low, 1986; Chanson, 1989;

(a)

(b)

Figure 1 Photographs of air–water flow at bottom outlet—Three Gorges Project on 20 October 2004, $V_0 = 35$ m/s, $Q = 1700$ m^3/s per outlet, $W_0 = 9$ m (per outlet). (a) General view from the dam crest. (b) Details (shutter speed: 1/1000 s)—flow from bottom left to top right.

Brattberg *et al.*, 1998, Tseng *et al.*, 1992; Kramer, 2004), but limited works included air–water velocity distribution measurements (Chanson, 1993; Brattberg *et al.*, 1998). To date, water jets past an abrupt drop have been little studied to date despite the relevance to bottom outlets.

1.2 Similitude and scale effect issues

Considering a water jet past an abrupt drop (Fig. 2), a simplified dimensional analysis yields a relationship between the air–water flow properties in the jet flow, the fluid properties and physical constants and inflow conditions:

$$C, \frac{F * d_0}{V_0}, \frac{V}{\sqrt{g * d_0}}, \frac{u'}{V_0}, \frac{d_{ab}}{d_0}, \cdots$$

$$= F_1\left(\frac{x}{d_0}; \frac{z}{d_0}; \frac{y}{d_0}; \frac{\delta}{d_0}; \frac{h}{d_0}; \frac{W_0}{d_0}; \frac{W}{d_0}; \right.$$

$$\left. \frac{V_0}{\sqrt{g * d_0}}; \frac{\rho * V_0 * d_0}{\mu}; \frac{u'_0}{V_0}; \frac{g * \mu^4}{\rho * \sigma^3}; \cdots \right) \quad (1)$$

where C is the void fraction, F the bubble count rate, V the velocity, g the gravity acceleration, d_0 the inflow depth at take-off, u' a characteristic turbulent velocity, V_0 the inflow velocity, d_{ab} a characteristic size of entrained bubble, x the coordinate
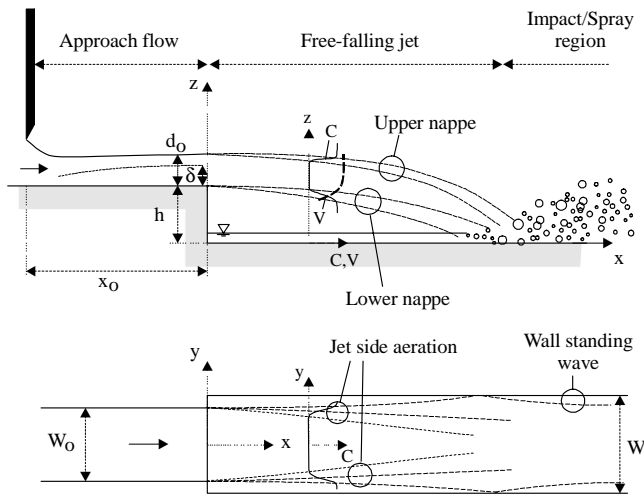
Figure 2 Definition sketch.

in the flow direction measured from the nozzle, z the vertical coordinate, y the transverse coordinate, δ the inflow boundary layer thickness, h the drop height, W_0 and W are the upstream and downstream channel widths, respectively, ρ and μ are the water density and dynamic viscosity, respectively, σ is the surface tension between air and water, and u'_0 is a characteristic turbulent velocity of the inflow (Fig. 2). On the right hand side of Eq. (1), the sixth and seventh terms are the inflow Froude and Reynolds numbers, respectively, while the ninth term is the Morton number that is a function only of fluid properties and gravity constant. In addition, biochemical properties of the water solution may be considered.

Despite some simplistic assumption, Eq. (1) demonstrates that dynamic similarity of free-surface aeration in a water jet is impossible with geometrically similar models because it is impossible to satisfy simultaneously Froude and Reynolds similarities. In small size models, the air entrainment process may be affected by significant scale effects. Wood (1991) and Chanson (1997, 2004) presented comprehensive reviews and illustrations. Basically dynamic similarity of interfacial aeration is dificult to achieve with geometrically similar models. Herein the investigations were performed in a relatively large-size facility operating with large flow Reynolds numbers (Table 1, column 8) to minimize potential scale effects.

2   Experimental apparatus and instrumentation

New experiments were performed in a 0.25 m wide channel ending with a free overfall (Table 1, Channel A). The flume was equipped with a 0.143 m high step located 0.62 m downstream of a vertical sluice gate. Additional work was conducted in another 0.5 m wide facility (Table 1, Channel B). Both channels had supercritical inflow conditions, i.e., $2 \leq Fr_0 \leq 10$, where Fr_0 is the approach flow Froude number. For all experiments, nappe ventilation was performed with sidewall offsets (Fig. 2). Cavity pressure measurements, using a projection manometer, demonstrated atmospheric pressures within 0.1 mm of water.

The water flow rates were measured with a V-notch weir calibrated on-site using a volume per time technique. The accuracy on discharge measurements was about 2%. Clear-water depths and velocities were measured with a point gauge and a Prandtl–Pitot tube (Ø = 3.3 mm), respectively. In the main facility, air–water flow properties were measured as double-tip conductivity probe (Ø = 0.025 mm) developed at the University of Queensland. The probe tips were aligned in the flow direction and excited by an air bubble detector (AS25240). The resistivity probe signals were scanned at 40 kHz for 40 s. In the second facility (Channel B), void fractions and bubble count rates were measured with a single-tip conductivity probe (Ø = 0.35 mm) scanned at 5 kHz for 180 s.

The translation of the probes in the vertical direction was controlled by a fine adjustment travelling mechanism connected to a Mitutoyo$^{\text{TM}}$ digimatic scale unit (Ref. Nos. 572–503). The error on the vertical position of the probe was less than $\Delta z < 0.025$ mm. The system (probe and travelling mechanism) was mounted on a trolley system. The accuracy on the longitudinal position of the probe was estimated as $\Delta x < 0.5$ cm. The accuracy on the transverse position of the probe was estimated as $\Delta y < 0.5$ mm. Further information and details were provided in Toombes (2002).

2.1   Approach flow conditions

In the main channel, the approach flow was controlled by a sluice gate. The measured contraction ratio was 0.66 ($\pm$5%) in average. At the abrupt drop, the flow was partially developed (Table 1,

Table 1 Experimental flow conditions

(1)	x_0 (m) (2)	h (m) (3)	W_0 (m) (4)	W (m) (5)	q (m^2/s) (6)	d_0 (m) (7)	Re (8)	δ/d_0 (9)	$(C_{\text{mean}})_0$ (10)	Comments (11)
Channel A	0.62	0.1433	0.237	0.250						Perspex step and glass flume
					0.084	0.0306	3.3 E+5	0.29	0.02	Run DT1
					0.097	0.0290	3.9 E+5	0.30	0.03	Run DT2
					0.111	0.0296	4.4 E+5	0.29	0.03	Run DT3
					0.087	0.0243	3.5 E+5	0.35	0.035	Run DT4
					0.143	0.0397	5.7 E+5	0.21	0.046	Run DT5
Channel B	2.4	0.1433	0.476	0.500	0.080–0.150	0.030	3.2–6E+5	1.0	0.07–0.12	Timber step and channel

Note: d_0: approach flow depth; h: step height; Re: Reynolds number defined in terms of hydraulic diameter; W: downstream channel width; W_0: approach channel width; x_0: approach channel length.

column 9). The depthaverage air concentration $(C_{\text{mean}})_0$ ranged from 0.02 to 0.04 for the investigated flow conditions, where C_{mean} is defined as

$$C_{\text{mean}} = \frac{1}{z_{90}} * \int_{y=0}^{z_{90}} C \, dz \qquad (2)$$

z is the distance normal to the invert and z_{90} is the characteristic air–water flow depth where $C = 0.90$. In the wide channel (Channel B), the flow was fed through a smooth convergent, the nozzle exit was 30 mm high, and the abrupt drop was located 2.4 m downstream. At the drop, the flow was fully developed and $(C_{\text{mean}})_0$ increased from 0.07 to 0.12 for flow rates between 0.080 and 0.150 m^2/s.

2.2 Experimental procedures

Initial air–water flow measurements showed that the inflow and free-falling jet were symmetrical around the channel centre-line. Air–water flow distributions were systematically measured at several longitudinal 4 locations x measured from the drop $(x/h = 0, 0.35, 0.7, 1.4, \ldots)$, on the channel centreline $(y = 0)$ and at several transverse locations y $(2 * y/W = 0, 0.4, 0.6 \ldots)$. Velocity measurements were performed with the Prandtl–Pitot tube in clear-water flow regions and with the dual-tip phase detection (conductivity) probe in the aerated flow regions.

3 Experimental results

For all investigated conditions, the flow may be divided into a number of regions that display distinctive characteristics, i.e., the approach flow, free-falling jet and impact region (Fig. 2). Downstream of the drop, a large air cavity was observed under the free-jet with atmospheric pressure for all experimental conditions. The flow was associated with significant air entrainment, which may be the cumulative result of a number of mechanisms. Namely (1) interfacial aeration in the approach flow region, and at the upper interface of the free-falling nappe, (2) bubble entrainment in the developing air–water shear layer at the lower interface of the free-jet, (3) plunging jet entrainment where the lower surface of the free-jet impacts into the pool of water beneath the nappe and (4) flow fragmentation at the impact of the nappe on the downstream invert, resulting in a significant volume of spray. Herein, the results are focused on the first two mechanisms.

At the lower nappe, an air–water free-shear layer developed downstream of the step brink. Experimental data showed that the amount of air entrained at the lower interface increased with distance from the step edge, as indicated by the thickness of the aerated region (Fig. 3a). In Fig. 3(a), centreline air-concentration profiles are shown for increasing distances from the edge of the step. The vertical axis is the dimensionless distance Z' centred about a point midway between the points of 50% air concentration at the upper and lower interfaces, i.e., $Z' = \left(z - \left(z_{50}^{\text{UpperNappe}} + z_{50}^{\text{LowerNappe}}\right)/2\right)/d_0$, X is the dimensionless horizontal distance from the drop $(X = x/d_0)$ and Y is the dimensionless transverse distance from the centreline
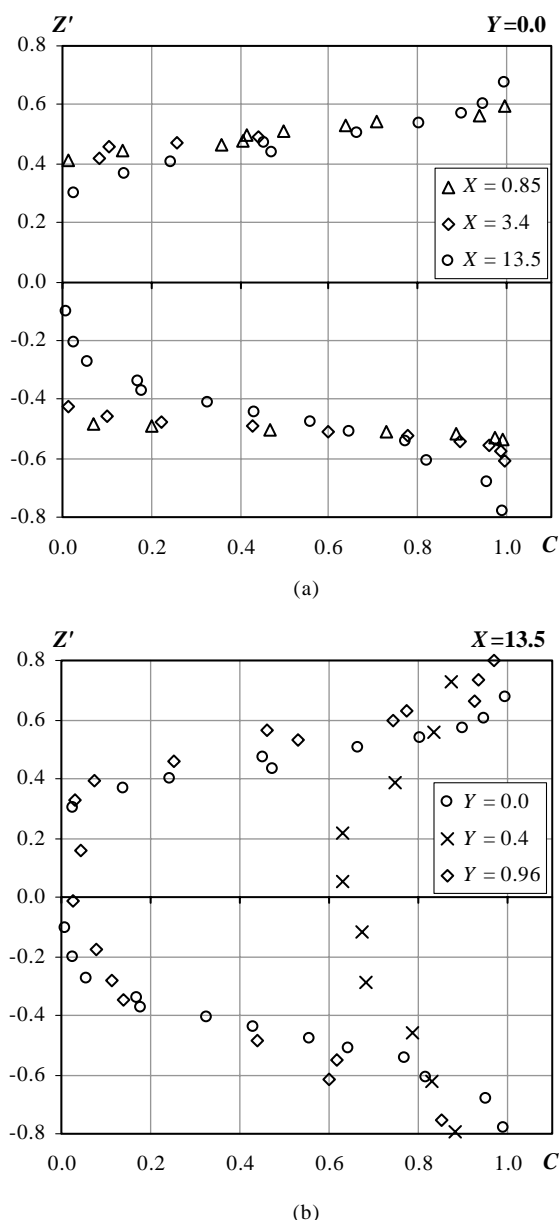

(a)

(b)

Figure 3 Dimensionless air concentration distributions in the free-jet—Run DT3, $d_0 = 0.0296$ m, $V_0 = 3.75$ m/s, Channel A. (a) Centreline data $(Y = 0)$: $X = 0.85$, 3.4 and 13.5. (b) Distributions for $X = 13.5$ at $Y = 0$, 0.4 and 0.96.

$(Y = 2 * y/W)$. At the upper interface, aeration was a combination of bubble entrainment in the air–water shear layer generated by the upstream sluice gate, free surface aeration and roughness of the free-surface. Although the amount of air entrainment increased with distance from the step edge, a slower rate was observed at the upper nappe compared with the lower nappe. Air was entrained into the jet at both upper and lower jet interfaces, as well as along the sides. Figure 3(b) shows air-concentration distributions for a series of sections across the nappe at a distance of 0.4 m downstream of the step edge for one experiment. While a clear-water (non-aerated) core exists at the jet centreline $(Y = 0)$, the time-average air concentration is greater than 0.60 across the entire thickness of the nappe in the section at $Y = 0.96$, clearly identifying the air entrainment at the sides of the free-falling jet.
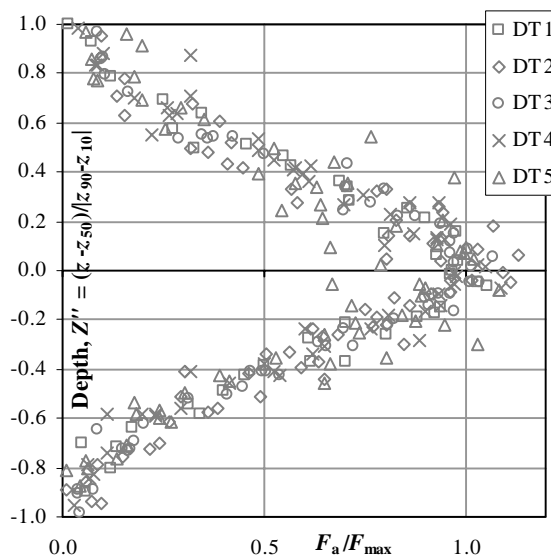
Typical bubble count rate distributions on the jet centreline are shown in Fig. 4(a). The bubble count rate is the number of air-bubbles or air-structures striking the leading probe tip per second. At the lower nappe, the maximum count rates were about three to five times greater than those observed at the upper interface. Further the maximum bubble count rate decreased with increasing distance from the step brink (Fig. 4(b)). In Fig. 4(b), dimensionless bubble frequency, $(\sigma/\rho * V^3) F_{max}$ is shown as a function of the longitudinal Weber number $We_x = \rho * V^2 * x/\sigma$, where V is the air–water velocity and F_{max} is the maximum bubble count rate in a section. For all investigated flow rates, maximum bubble count data were best correlated by

$$\frac{\rho * F_{max}}{\rho * V^3} = \left(0.11 * \frac{\rho * V^2 * x}{\rho} + 610\right)^{-1} \quad \text{Lower nappe (3)}$$

Typical centreline velocity profiles through the free jet are shown in Fig. 5. Data from both double-tip conductivity probe and Pitot tube are shown. The Pitot tube was accurate in the non-aerated core of the jet, but its accuracy was severely reduced in the air–water interface. The double-tip conductivity probe was

	DT1	DT2	DT3	DT4	DT5
d_0 (m)	0.0306	0.0290	0.0296	0.0243	0.0397
V_0 (m/s)	2.76	3.35	3.75	3.59	3.61

(a)
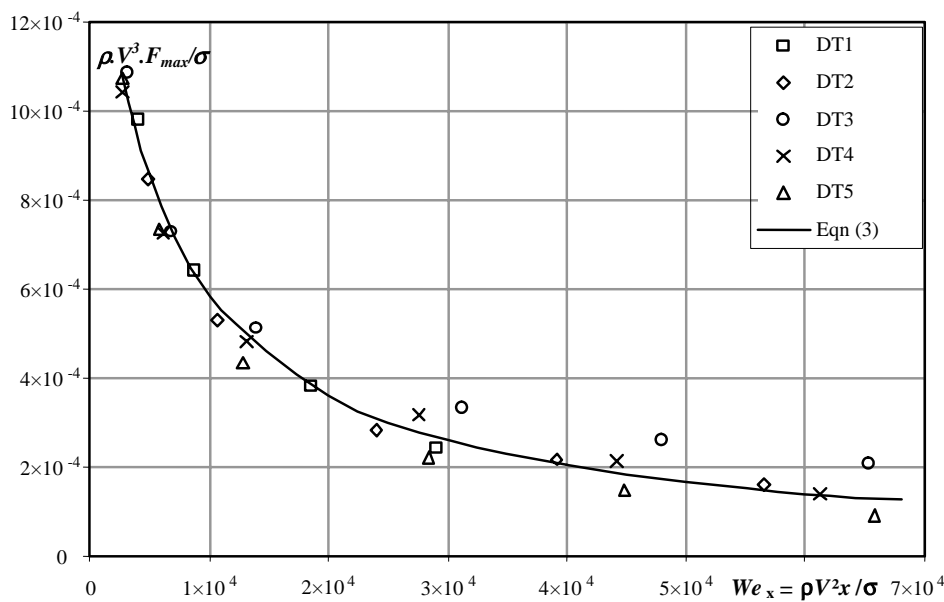
(b)

Figure 4   Bubble count rate distributions in the free-jet (Channel A). (a) Dimensionless distributions of bubble count rate at the lower interface. (b) Longitudinal variation of the dimensionless maximum bubble count rate at the lower interface—comparison with Eq. (3).
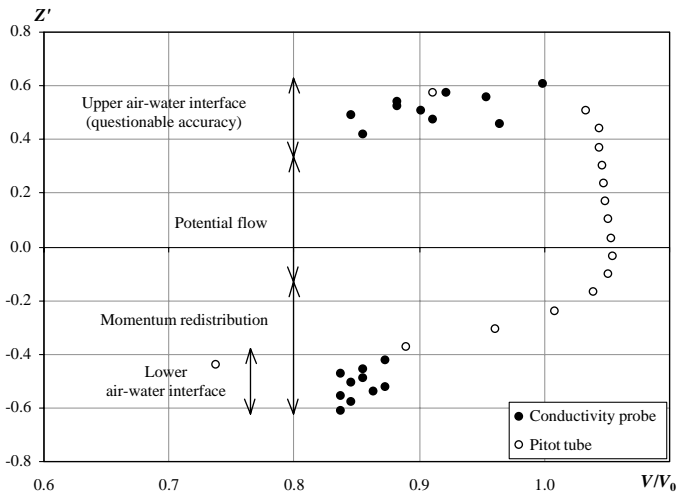
Figure 5 Air–water velocity distribution in the free-jet—Run DT3, $d_0 = 0.0296$ m, $V_0 = 3.75$ m/s, $X = 3.4$.

only useful in the air–water mixture flow. As shown in Fig. 5, the velocity at the middle of the jet was reasonably constant (potential flow), and increased with distance downstream of the step brink as the falling jet accelerated under gravity. Lesser velocities were observed at the lower nappe interface. This was quite likely caused by the developing turbulent boundary layer in the approach channel, which reduced the velocity close to the channel invert, upstream of jet take-off. At the upper nappe interface, conductivity probe velocity data showed a significant scatter, which derived from relatively low cross-correlation between the two tip signals (Toombes, 2002).

Dimensionless pressure distributions through the free-falling nappe are shown in Fig. 6, where P_{max} is the maximum pressure detected at each section (relative to atmospheric) and Z' is the dimensionless height. The data were deduced from Pitot tube readings. They were reasonably well represented by a parabolic distribution, tending to atmospheric at both the upper and lower surfaces, although there was some scatter. While some points may be "bad data" (e.g. air-bubbles trapped in Pitot tube tapping), evidence suggested that the pressure within the nappe was fluctuating over time. Pressure distributions in a free jet were investigated previously (Rouse, 1936; Henderson, 1966). With a ventilated cavity, the pressure above and below the nappe must be atmospheric, but the pressure within the nappe is not necessarily atmospheric. Rouse (1936) stated that considerable internal pressure still exists within the nappe, caused by the convergence of the streamlines between the upper and lower surfaces of the nappe. Present results showed little longitudinal variations in pressure at the centre of the nappe with distance from the step brink. The maximum measured pressures at each section were typically $P_{max}/(\rho * g * d_0) = 0.6-0.7$. Since the inflow was supercritical, there was no significant contraction of the nappe with distance, and this could possibly explain the little longitudinal variations.

4 Interfacial aeration and momentum exchange

4.1 Air diffusion

In a high-velocity water jet discharging into the atmosphere, Chanson (1989, 1997) developed an analytical solution of the
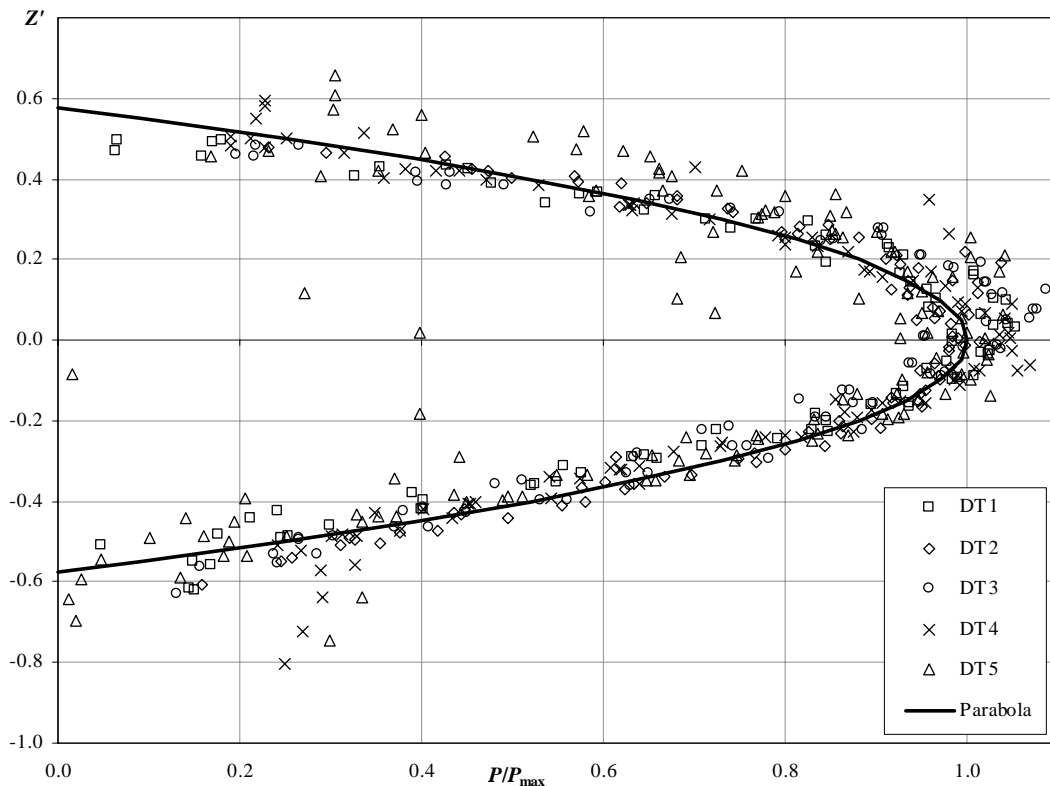

Figure 6 Dimensionless pressure distributions in the free-jet.

advective diffusion equation for air bubbles, which may be rewritten as

$$C = \frac{1}{2} * \left(1 + \mathrm{erf} \left(\frac{z - z_{50}}{2 * \sqrt{D_t * \frac{x}{V_0}}} \right) \right) \quad \text{Upper nappe} \quad (4a)$$

$$C = \frac{1}{2} * \left(1 + \mathrm{erf} \left(\frac{z_{50} - z}{2 * \sqrt{D_t * \frac{x}{V_0}}} \right) \right) \quad \text{Lower nappe} \quad (4b)$$

where D_t is the turbulent diffusivity assumed independent of the normal direction z, z_{50} is the location where $C = 0.5$ and erf is the Gaussian error function. Equation (4) is an analytical solution assuming that the turbulence is homogeneous, the buoyancy effects are negligible and a clear-water core prevents interaction between upper and lower nappe entrainment. Equations (4a) and (4b) are compared with present data in Fig. 7, where $Z'' = (z - z_{50})/(z_{90} - z_{10})$, and z_{10} and z_{90} are locations where $C = 0.10$ and 0.90, respectively. The results demonstrate the self-similarity of the data. The good agreement indicates further that D_t was approximately constant in the vertical direction, but experimental results showed that D_t increased with increasing distance from the brink. The trend was consistent with a re-analysis of the data of Low (1986), Chanson (1989) and Brattberg *et al.* (1998). The findings showed that the turbulent diffusivity was best correlated by

$$\frac{D_t}{v} = K * \frac{\rho * V^2 * x}{\sigma}$$
$$\text{Lower nappe } (3E+3 < We_x < 8\,E+5) \quad (5)$$

where v is the water kinematic viscosity. Equation (5) is based upon the analysis of the data from Low (1986), Chanson (1989), Brattberg *et al.* (1998) and the present study. Despite some scatter, the majority of the data formed a band between $1\,E-3 < K < 3\,E-3$, with a mean value of $K = 1.5\,E-3$. The relatively close agreement of all data was unexpected considering the differences in experimental flow conditions and geometries.

4.2 Momentum redistribution in the jet

Figure 8 illustrates the velocity redistribution in the high-velocity air–water jet, where V_p is the velocity of the potential (uniform) flow region of the jet and x is measured in metres. Both Pitot tube and double-tip conductivity probe data are shown. At the upper air–water interface, there was negligible momentum exchange between the flow and the atmosphere (Toombes, 2002). The inflow conditions were partially developed with a "potential" flow region above the boundary layer. This ideal-fluid flow region was maintained in the upper layer of the free-jet, with the velocity increasing along the jet due to gravitational acceleration. The ideal fluid flow velocity was predicted using the Bernoulli equation and the equations of motion with an error of less than 1%. At the lower nappe, the velocity profiles showed a distinct change as the distance from the step brink increased. Immediately downstream of the drop, the velocity profile at the lower interface had a profile similar to that observed in a turbulent boundary layer.

The velocity profile became more uniform across the jet as the distance from the drop increased.

For a water jet discharging into air, the air velocity at the air–water interfaces must be equal to the velocity of the water. Hence a transfer of momentum from the water jet is required to accelerate the air. Dodu (1957) found that the thickness of the mobilized air layer is relatively small. Assuming that the volume of air mobilized is of similar magnitude as the volume of water, and given that the air starts at rest and has a final velocity equal to that of the water, the change in water jet velocity must be around 0.12% of the initial jet velocity, and the magnitude of the momentum lost by the water is negligible (over a short distance). For the present investigation, and within the accuracy of the instrumentation, the momentum flux along the water jet J_w ($0 \le x/d_0 \le 15$) was calculated as

$$J_w = \int \rho * (1 - C) * V^2 \, \mathrm{d}z \quad (6)$$

where V and C are the measured velocity and time-averaged air concentration at elevation z. Present results demonstrated that there was basically no loss of momentum from the water jet along its trajectory.

4.3 Wake flow region at the lower nappe

In the approach channel, the turbulent boundary layer is a zone affected by a shearing force from friction at the invert. Downstream of the drop, the shearing force at the lower interface is zero. The internal viscous shear forces within the fluid result in a redistribution of the velocity profile along the jet. It is possible to model the velocity redistribution within the jet, assuming a monophase liquid jet discharging into a void, i.e., neglecting air entrainment at the air–water interface and transfer of momentum from the jet to the air. For a homogenous, steady-state, incompressible fluid, the Navier–Stokes and continuity equations can be written for a two-dimensional turbulent free-jet as

$$\frac{\partial V_x}{\partial x} + \frac{\partial V_z}{\partial z} = 0 \quad \text{[Continuity]} \quad (7a)$$

$$V_x * \frac{\partial V_x}{\partial x} + V_z * \frac{\partial V_x}{\partial z} = \frac{1}{\rho} * \frac{\partial \tau}{\partial z} \quad \text{[Momentum]} \quad (7b)$$

where V_x and V_z are the velocity components in the x and z directions and τ is the shear stress, which may be derived from Prandtl mixing length hypothesis as

$$\tau = \rho * v_T * \frac{\partial V_x}{\partial z} \quad (8)$$

v_T is the momentum exchange coefficient assumed independent of z expressed as $v_T = \gamma * b * V_0$, γ is an empirical constant and b is the width of the mixing layer (Goertler, 1942; Schlichting, 1979). Given the complexity of the inflow conditions (uniform flow above a turbulent boundary layer) and the boundary conditions of the jet (zero shear stress at the air–water interfaces), it is impossible to solve the Navier–Stokes and continuity equations analytically. Instead a numerical model was developed to predict the change in velocity (Toombes, 2002). The results demonstrated that the numerical integration predicted well the
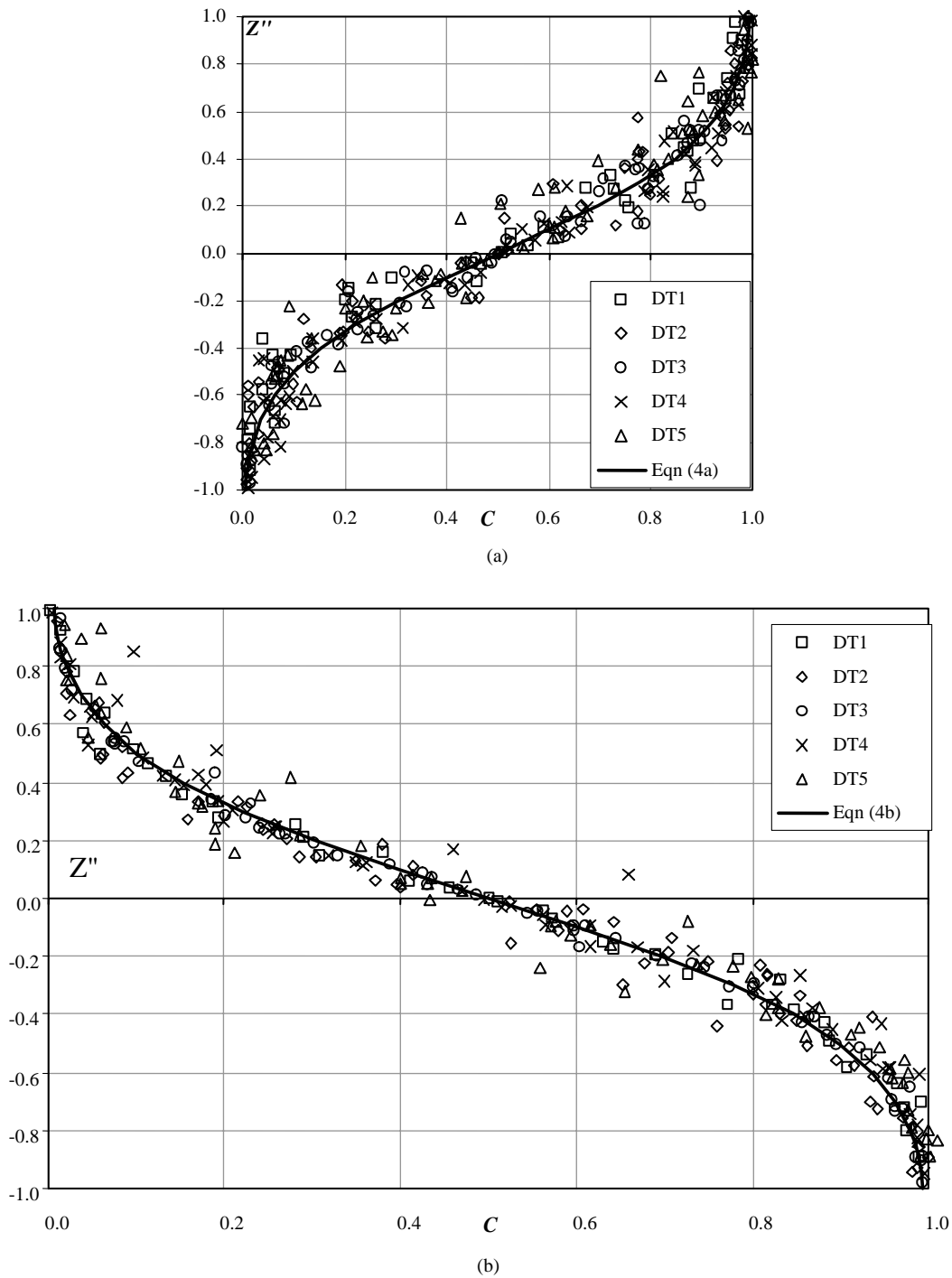
(a)

(b)

Figure 7   Dimensionless air concentration distributions: (a) Upper nappe data—comparison with Eq. (4a). (b) Lower nappe data—comparison with Eq. (4b).

measured velocity profiles. A sample output from the model is shown in Fig. 8.

The boundary conditions for a jet of semi-infinite thickness discharging into a void are similar to the boundary condition for wake flow behind a symmetrical bluff body. Analytical solutions for two-dimensional wake flows can be developed in the far wake region downstream

$$\frac{V}{V_0} = 1 - \frac{K'}{\sqrt{x}} * \exp\left(-\frac{V_0 * z^2}{4 * v_{\mathrm{T}} * x}\right) \tag{9}$$

where K' is an integration constant determined to satisfy continuity (Goertler, 1942; Schetz, 1993). Equation (9) showed a good agreement with both numerical model and experimental data, although the assumptions upon which Eq. (9) is based (far wake $(1 - V/V_0) \approx 1$) limit the range of the jet over which it can be accurately applied. It must be noted that both analytical and numerical solutions were developed for monophase flow, and they did not implicitly account for interfacial aeration. The output from both models can be adapted to account for air entrainment by adjusting the scaling of the vertical direction to account for flow bulking. The continuity equation across a small distance yields:
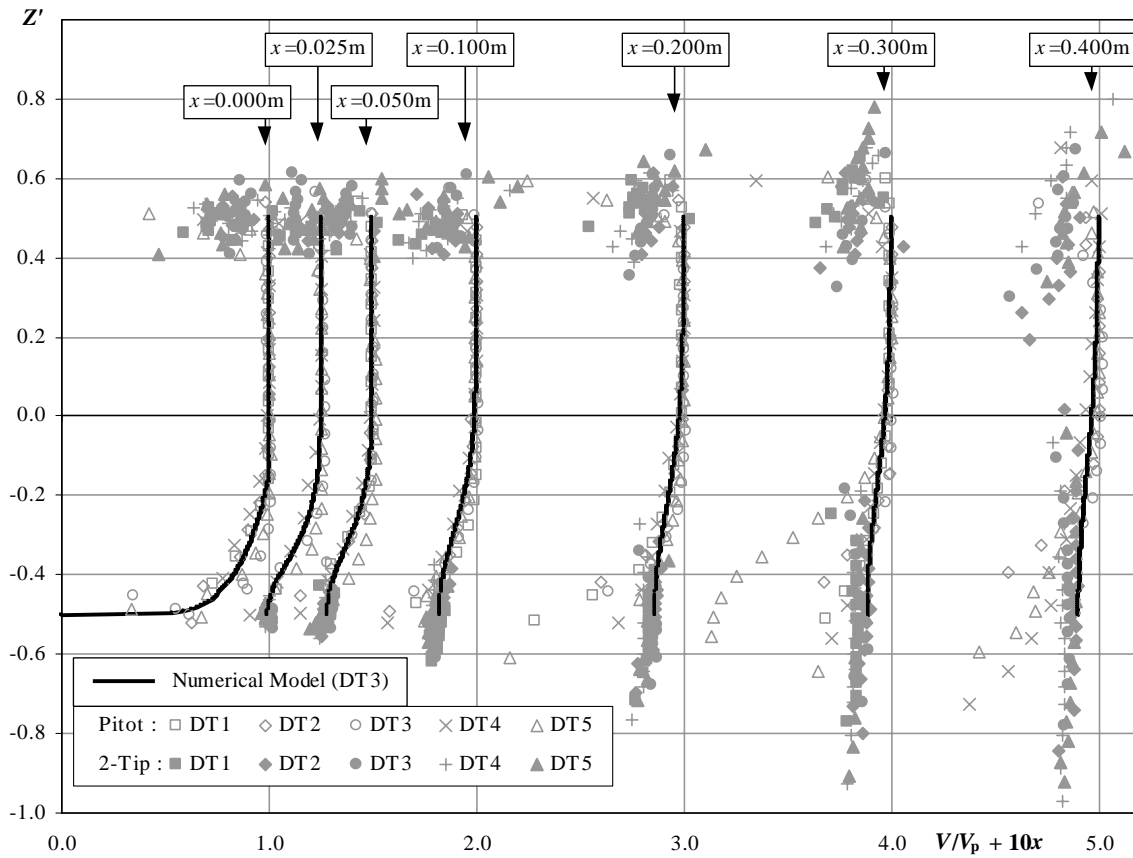
Figure 8   Dimensionless velocity distributions through the free-jet — comparison between experimental data and numerical analysis.

$dz' = dz/(1 - C)$, where z is the vertical coordinate assuming no air entrainment and z' is the modified coordinate.

Based upon the measured air–water velocity distributions, the momentum exchange coefficient was estimated for the investigated flow conditions. A good agreement with the experimental data was obtained, as demonstrated in Fig. 8, assuming that the eddy viscosity was of the order of $v_T/v = 400$. Basically the momentum exchange coefficient was found to be independent of the longitudinal location (within $0 \leq X < 15$) and inflow conditions. Since the velocity profiles at the lower nappe were reasonably well estimated by the wake flow model, the finding refutes the hypothesis of Chanson (1993, 1997) of a free-shear layer flow.

5   Discussion

Downstream of the step, the free-jet was subjected to both significant interfacial aeration and velocity redistribution. Close to the step brink ($We_x < 5000$), the air bubble turbulent diffusivity was significantly smaller than the momentum exchange coefficient, i.e., $D_t/v_T < 0.02$. The turbulent diffusivity increased almost linearly with the distance from the step brink (Eq. (5)). Consequently, upstream of nappe impact ($5E+3 < We_x < 5E+4$), the turbulent diffusivity was almost of the order of magnitude of the eddy viscosity, i.e., $D_t/v_T \sim 0.2-0.5$. A re-analysis of existing data, presented in Chanson (1997), derived the ratio of turbulent diffusivity to eddy viscosity for a range of experiments,

including two-dimensional plunging jets, two-dimensional water jets and open channel flows. Results were typically of the order $0.2 < D_t/v_T < 3$. That is, present results for $We_x > 5E+3$ fall within this range.

The ratio of bubble diffusivity to eddy viscosity D_t/v_T compares the effects of the difference in diffusion of a discrete bubble particle and small coherent fluid structure, as well as the effect of entrained air on the turbulence field. Close to the step brink ($We_x < 5000$), present result (i.e. $D_t/v_T < 0.02$) seem to suggest that momentum exchange processes are dominant. Further downstream ($5E+3 < We_x < 5E+4$), the results (i.e. $D_t/v_T \sim 0.2-0.5$) imply strong competition between the air bubble diffusion and momentum exchange processes. The presence of large amounts of entrained air is expected to modify some turbulence characteristics while the turbulence controls the mechanism of bubble break-up and the air–water interfacial properties. For longer jets (i.e. $We_x > 5E+4$), present results would imply that the ratio D_t/v_T become large and the jet flow be dominated by interfacial aeration. This would yield to jet breakup and disintegration discussed by Kawakami (1973) and Ervine and Falvey (1987).

However, there are a number of issues regarding both the estimate of the momentum exchange coefficient and any comparison between v_T and D_t that must be considered (Toombes, 2002). For example, it could possibly be argued that the estimate of mixing layer thickness used in the above calculations underestimated (or overestimated) the mixing layer thickness, while the effects of air entrainment on the eddy viscosity were unknown. Further the

air–water mixing layer thickness was initially significantly less than the width of the momentum mixing layer, but increased significantly with distance from the step brink. The increase in the width of the air–water mixing layer relative to the momentum mixing layer was most likely responsible for the growth in D_t observed.

6 Summary and conclusion

Interfacial aeration and momentum transfer were investigated experimentally in a supercritical flow past an abrupt drop, typical of some bottom outlet configurations (Fig. 1). Downstream of the step brink, the free-jet entrains large amounts of air at both upper and lower air–water interfaces, as well as along the sides. An air–water shear layer develops at the lower nappe interface. Measured air-concentration distributions within the shear layer showed good agreement with an analytical solution of the basic diffusion equation for air-bubbles, based on the continuity equation for air (Eq. (4), Fig. 7). Present data, together with the re-examination of previous experimental studies, suggested that the air-bubble turbulent diffusivity increased with increasing distance from the singularity point (i.e. step brink).

The turbulent boundary layer upstream of the step brink was partially developed. Downstream of the brink, friction forces from the step invert were no longer present and the velocity field at the lower nappe was subjected to a strong redistribution. Experimental results showed a negligible loss of momentum from the free-falling jet to the surrounding air. The velocity redistribution within the jet was successfully modelled by integrating numerically the Navier–Stokes and continuity equations. Beyond a certain distance from the step brink, the velocity field was found to be similar to that in two-dimensional wake flow, and it was reasonably well estimated by analytical solutions for the "far-wake region" (Eq. (9), Fig. 8). The results highlighted two distinct flow regions. Close to the brink ($We_x < 5000$), the flow was dominated by momentum transfer as the result of the step brink singularity. Further downstream ($We_x > 5000$), the results implied a strong competition between air bubble diffusion and momentum exchanges.

In practice, the flow conditions are closely linked with the geometry of the bottom outlet (e.g. h, W, W_0). These were not systematically studied herein and further investigations should be pursued.

Notation

C = Air concentration

C_{mean} = Depth-averaged air concentration

D_t = Air bubble diffusivity (m²/s)

d = (1) flow depth (m) measured normal to the invert
(2) equivalent clear-water flow depth (m): $d = \int_0^{z_{90}} (1 - C)\, dz$

d_0 = Approach flow depth (m)

F = Bubble count rate (Hz) defined as the number of bubbles impacting the probe tip per second

F_{max} = Maximum bubble count rate (Hz) in a section

Fr = Froude number defined as $Fr = V/\sqrt{g*d}$

Fr_0 = Inflow Froude number

g = Gravity constant (m/s²) or acceleration of gravity

h = Height of drop (m) (measured vertically)

J_w = Momentum flux per unit width (kg/s²)

K, K' = Dimensionless constants

P = Pressure (Pa)

P_{max} = Maximum pressure (Pa) in a section

Q = Water discharge (m³/s)

q = Water discharge per unit width (m²/s)

Re = Reynolds number

V = Velocity (m/s)

V_0 = Inflow velocity (m/s)

V_x = Longitudinal velocity component (m/s)

V_z = Vertical velocity component (m/s)

W = Downstream channel width (m)

W_0 = Approach channel width (m)

We_x = Longitudinal Weber number $We_x = \rho * V^2 * x/\sigma$

X = Dimensionless longitudinal distance $X = x/d_0$

x = Longitudinal distance (m) measured in the step vertical face

x_0 = Approach flow channel length (m)

Y = Dimensionless transverse distance $Y = 2 * y/W$

y = Transverse distance (m) measured from the channel centreline

z_{10}, z_{50}, z_{90} = Vertical distance (m) measured from the step invert where $C = 0.10, 0.50, 0.90$

Z = Dimensionless vertical distance $Z = z/d_0$

Z' = Centred dimensionless distance $Z' = \left(z - (z_{50}^{\text{UpperNappe}} + z_{50}^{\text{LowerNappe}})/2\right)/d_0$

Z'' = Dimensionless coordinate $Z'' = (z - z_{50})/(z_{90} - z_{10})$

z = Vertical distance (m) measured from the step invert

z' = Modified vertical coordinate (m)

Greek symbols

δ = Boundary layer thickness (m)

γ = Dimensionless constant

υ = Kinematic viscosity of water (m²/s)

V_T = Momentum exchange coefficient (m²/s)

ρ = Water density (kg/m³)

σ = Surface tension of air and water (N/m)
τ = Shear stress (Pa)

Subscript

0 = Approach flow conditions
x = Longitudinal component
z = Vertical component.

References

1. BRATTBERG, T., CHANSON, H. and TOOMBES, L. (1998). "Experimental Investigations of Free-Surface Aeration in the Developing Flow of Two-Dimensional Water Jets". *J. Fluids Eng., Trans. ASME* 120(4), 738–744.

2. CHANSON, H. (1989). "Study of Air Entrainment and Aeration Devices". *J. Hydraul. Res., IAHR* 27(3), 301–319.

3. CHANSON, H. (1993). "Velocity Measurements within High Velocity Air-Water Jets". *J. Hydraul. Res., IAHR* 31(3), 365–382 and (6), 858.

4. CHANSON, H. (1997). *Air Bubble Entrainment in Free-Surface Turbulent Shear Flows*. Academic Press, London, UK.

5. CHANSON, H. (2004). *Environmental Hydraulics of Open Channel Flows*. Elsevier Butterworth-Heinemann, Oxford, UK.

6. DODU, J. (1957). "Etude de la Couche Limite d'Air autour d'un Jet d'Eau à Grande Vitesse". *Proceedings of the 7th IAHR Congress*, Lisbon, Portugal, paper D6.

7. ERVINE, D.A. (1998). "Air Entrainment in Hydraulic Structures: A Review". *Proceedings of the Institution of Civil Engineers, Water, Maritime & Energy*, UK, Vol. 130, September, pp. 142–153.

8. ERVINE, D.A. and FALVEY, H.T. (1987). "Behaviour of Turbulent Water Jets in the Atmosphere and in Plunge Pools". *Proceedings of the Institution of Civil Engineers, London*, Part 2, March 1987, Vol. 83, pp. 295–314. Discussion: Part 2, March–June 1988, Vol. 85, pp. 359–363.

9. GOERTLER, H. (1942). "Berechnung von Aufgaben der freien Turbulenz auf Grund eines neuen Näherungsansatzes". *Z.A.M.M.* 22, 244–254 (in German).

10. HENDERSON, F.M. (1966). *Open Channel Flow*. MacMillan Company, New York, USA.

11. HERAUD, D. (1966). "Dispersion des Jets Liquides: Influence des Rugosités de Paroi". PhD Thesis, University Grenoble 1, France.

12. KAWAKAMI, K. (1973). "A Study of the Computation of Horizontal Distance of Jet Issued from Ski-Jump Spillway". *Proc. JSCE* 219(11), 37–44 (in Japanese).

13. KRAMER, K. (2004). "Development of Aerated Chute Flow". PhD Thesis, VAW, ETH-Zürich, Switzerland.

14. LOW, H.S. (1986). "Model Studies of Clyde Dam Spillway Aerators". Research Report No. 86-6, Department of Civil Engineering, University of Canterbury, Christchurch, New Zealand.

15. NOVAK, P., MOFFAT, A.I.B., NALLURI, C. and NARAYANAN, R. (2001). "Hydraulic Structures". Spon Press, London, UK.

16. ROUSE, H. (1936). "Discharge Characteristics of the Free Overfall". *Civil Eng.* 6(April), 257.

17. SCHLICHTING, H. (1979). Boundary Layer Theory. 7th edn. McGraw-Hill, New York, USA.

18. SCHETZ, J.A. (1993). Boundary Layer Analysis. Prentice Hall, Englewood Cliffs, USA.

19. SHI, Q., PAN, S., SHAO, Y. and YUAN, X. (1983). "Experimental Investigation of Flow Aeration to Prevent Cavitation Erosion by a Deflector". *Shuili Xuebao (J. Hydraul. Eng.)*, Beijing, China, 3, 1–13 (in Chinese).

20. SPEERLI, J. (1999). "Stomungsprozesse in Grundsblassstolen". PhD Thesis, VAW, ETH-Zurich, Switzerland.

21. TOOMBES, L. (2002). "Experimental Study of Air-Water Flow Properties on Low-Gradient Stepped Cascades". PhD Thesis, Department of Civil Engineering, The University of Queensland.

22. TSENG, L.K., RUFF, G.A. and FAETH, G.M. (1992). "Effects of Gas Density on the Structure of Liquid Jets in Still Gases". *AIAA J.* 30(6), 1537–1544.

23. VISCHER, D. and HAGER, W.H. (1998). Dam Hydraulics. John Wiley, Chichester, UK.

24. WOOD, I.R. (1991). *Air Entrainment in Free-Surface Flows*. IAHR Hydraulic Structures Design Manual No. 4, Hydraulic Design Considerations, Balkema Publ., Rotterdam, The Netherlands.